Mapping of Elastic Modulus and Hardness in *Trochus niloticus* Seashell Nacre by Nanoindentation

by

Julián Enrique Villarreal

Submitted to the Department of Materials Science and Engineering
in Partial Fulfillment of the Requirements
for the Degree of

Bachelor of Science

at the

Massachusetts Institute of Technology

June 2007

Signature of Author.....
Department of Materials Science and Engineering
May 22, 2006

Certified by.....
Christine Ortíz
Associate Professor of Materials Science and Engineering
Thesis Supervisor

Accepted by.....
Caroline Ross
Professor of Materials Science and Engineering
Chair, Departmental Undergraduate Committee

MAPPING OF ELASTIC MODULUS AND HARDNESS

IN *TROCHUS NILOTICUS* SEASHELL NACRE

BY NANOINDENTATION

by

JULIÁN ENRIQUE VILLARREAL

Submitted to the Department of Materials Science and Engineering
on May 22, 2006 in partial fulfillment of
the requirements for the Degree of Bachelor of Science in
Materials Science and Engineering

ABSTRACT

Positionally-sensitive nanoindentation was carried out in the freshly-cleaved nacre found in the shell of the gastropod mollusk *Trochus niloticus*. Nacre is a hierarchical biocomposite composed of mineral tablets of 95 weight % calcium carbonate ($CaCO_3$) in the aragonite mineral form and a biomacromolecular organic matrix. Nanoindentation was carried out in a pattern of square grids of 256 indents at maximum loads of 1 mN and 500 μN. The average elastic modulus and hardness for the 1 mN indents were found to be 97.8 GPa ± 6.41 GPa and 5.41 GPa ± 0.49 GPa, respectively, and for the 500 μN indents average elastic modulus of 94.8 GPa ± 7.28 GPa and hardness of 4.89 GPa ± 0.53 GPa. Maps of the 2-D spatial distribution of elastic modulus and hardness for the indent areas were generated. Tapping mode Atomic Force Microscopy was performed on the indented nacre after a treatment of surface etching, which revealed the tablet boundaries in order to correlate qualitatively the topographical features with the properties distribution. The properties distribution maps revealed a non-uniform distribution of nanomechanical properties as well as highly-localized regions in which the values of the properties differed from the average values. Future studies may point to a direct correlation between structural heterogeneity and the properties distribution.

Thesis Supervisor: Christine Ortíz

Title: Associate Professor of Materials Science and Engineering

TABLE OF CONTENTS

I. Introduction

Biological materials are of great interest to materials science because of the inherent complexity, order, and self-assembly of biological systems. The nacre of mollusk shells, for example, is a biological composite material that exhibits a hierarchical architecture[1]. A hierarchically structured material has important features at multiple length scales, and multiscale characterization of these materials must be carried out to gain a full-spectrum understanding of their properties and structure[2]. It is believed that the structural heterogeneity of nacre confers strong mechanical performance because of variety of deformation mechanisms that in combination yield high energy-absorbing qualties[1]. This investigation seeks to map the two-dimensional (2-D) spatial distribution of Elastic Modulus and Hardness as a function of indent position on the microtablets of *Trochus niloticus* seashell nacre. Determining the properties distribution will shed further light on the nanomechanical properties of key structural features. Future nacre-like materials would need to simulate the nanomechanical properties distribution in order to mimic fully the mechanical performance of nacre.

A. Background

The conical shell of the gastropod mollusk, *Trochus niloticus*, contains an inner nacreous layer. This nacreous material is found in the bottom walls of the inner chamber, beneath a prismatic layer (Figure 1). Previous studies of nacre show that it is composed of layers of pseudohexagonal, polygonal, and rounded aragonite mineral tablets (95 weight % orthorhombic $CaCO_3$) arranged in a brick-and-mortar fashion, with a biomacromolecular organic matrix occupying the inter-tablet region[3] (Figure 2). These mineral tablets have dimensions ranging from 5 μm to 15 μm along the a- and b-axes ([100] and [010] crystallographic directions, respectively) and about 0.3-1.5μm along the direction parallel

to the c-axis ([001] direction)[3,4]. Scanning electron microscopy (SEM) and Atomic Force Microscopy (AFM) reveal that each tablet has a distinct nucleation site at its center from which tablet sectors radiate[1]. The tablet sectors are thought to be individual crystals of aragonite that are separated by the organic matrix[5,6]. The mineral tablets differ in the number and relative size of the sectors, each tablet typically having between two and ten sectors. Protein studies of the organic matrix suggest that glysine-rich structural motifs may be necessary to Ca^{2+} binding for tablet nucleation[7]. The nanoscale morphology of the surface of the tablets (the (001) crystallographic plane) consists of nanoasperities[1]. In *California red abalone* nacre, these nanoasperities are 30-100 nm in diameter and about 10 nm in height[8]. High-resolution Tapping Mode AFM (TMAFM) amplitude images reveal the presence of polymer fibrils in the valleys between neighboring nanoasperities[1].

A. P. Jackson, et al. have previously characterized the continuum mechanical properties of nacre. The average elastic modulus is has been found to range from 60 GPa to 80 GPa[9,10], as determined by various methods of mechanical testing, including uniaxial compression. It is useful to note for the sake of comparison that the elastic modulus of purely crystalline aragonite is 76-144 GPa depending on the orientation[11], while that of low-carbon steel is 200 GPa and that of aluminum is 68 GPa. Previous nanoindentation studies of *T. niloticus* nacre have shown the modulus to range from 70 GPa to 100 GPa[1]. It should be noted, however, that the nanomechanical properties of the nacre often vary. These variations are due in part to the differing mechanical responses of nano- and microscale structural features (e.g. tablet boundaries, nucleation sites, etc.)[1].

B. Motivations and Methodology

The ultimate goal of this investigation is to deepen the understanding of the nano- and microscale mechanical performance of nacre and to learn from nature. Natural

selection has driven the evolution of nacre and has harnessed the principles of hierarchical design in order to extract robust mechanical performance from constituent materials that do not exhibit particularly good mechanical properties in their native state. A fuller understanding of nanomechanical performance in nacre will make possible the development of materials and technology that can mimic the mechanical behavior of biocomposites (biological organic-inorganic composite materials), such as nacre. The energy-absorbing abilities of nacre, in particular, are of great interest. For example, nacre has a fracture toughness ranging from 2.9 to 5.7 MPa·$\sqrt{m}$[9], compared to that of aragonite, which ranges from 0.1 to 0.2 MPa·$\sqrt{m}$[11].

The following issues were addressed in this investigation: what is the topographical distribution of elastic modulus and hardness as a function of indent position on the mineral tablets, and how does one develop a method for correlating indent position and topographical features? In order to answer these questions, the following methodology was used: (1) Positionally-sensitive nanoindentation in a square grid of indents was carried out in the freshly-cleaved nacre of *T. niloticus*; (2) the values for the elastic modulus and hardness for each indent curve were determined and (3) these values were used to produce elastic modulus and hardness maps of the 2-D topographical distribution of these properties over the indented area.

II. Materials and Methods

A. Sample Preparation

Nacre samples were cut from shells of mature *Trochus niloticus* (purchased from Shell Horizons, Clearwater, FL). The shells were cut using a diamond-impregnated circular saw (Buehler, Isomet 5000) at a blade speed of 975 rpm and cooled with a PBS-buffered water solution (pH 7.3). Slices of nacre were harvested from the inner nacreous

chamber walls (Figure 1). These slices were then cleaned and sonicated in de-ionized water for 10 minutes with an Ultramet ultrasonic cleaner. All samples used for nanoindentation were cleaved in uniaxial compression in ambient conditions using a Zwick-Roell mechanical tester (Model BTC-FR010TH.A50, 10-kN maximum load cell, 0.01 mm/min), with axis of loading parallel to the tablet layers (i.e. perpendicular to the aragonite c-axis, Figure 3). This method of preparation produced cleavage between the tablet layers, leaving a flat surface for nanoindentation. A sample was considered "freshly-cleaved" if it was used within one hour of cleavage by uniaxial compression.

B. Nanoindentation

A *Hysitron, Inc.* ® Triboindenter nanoindenter was used to conduct nanoindentation experiments in ambient conditions. A trigonal pyramidal Berkovich diamond probe tip was employed for all calibrations and nanoindentation experiments. Experiments were carried out at two maximum loads, 1 mN and 500 μN, at a loading rate of 50 μN/s. A square grid of 16 indents on each side was set as the indentation pattern for a total of 256 indents per grid. Neighboring indents were separated by at least two microns on each side, for the 1 mN indents, and by at least one micron for the 500 μN indents. The entire grid, therefore, covered an area of 900 sq. μm (30 μm x 30 μm) for the 1 mN indents and 225 sq. μm (15 μm x 15 μm) for the 500 μN indents. Four large positioning indents were also done at a maximum load of 10 mN in a square grid of 25 μm x 25 μm for the 500 μN indents and a grid of 35 μm x 35 μm for the 1 mN indents in order to facilitate locating of the indents upon AFM imaging. Nanoindenter operating parameters are given in section A of the Appendix. Values for the elastic modulus were calculated by means of Oliver-Pharr (O-P) analysis of the nanoindentation curves[12]. The parameters for the O-P analysis can be found in the Appendix.

C. Surface Etching and Alteration

A surface alteration method employing acid-base etching was developed in order to reveal the tablet boundaries and other features, such as the biomineralization nucleation sites and sector lines, and the position of these features relative to indents. Once the nacre was indented, the sample was treated in order to partially deorganify the nacre. This method of treatment was developed because the presence of the organic matrix occludes the tablet features to a certain degree depending on the sample surface texture and quality, which can vary even among different areas on a same nacre sample. It has been previously determined that the concentration of organic matrix is highest in the region of the nucleation site, in the region between tablets (heretofore referred to as the tablet boundaries) and between tablet sectors (heretofore referred to as sector lines)[1]. The surface etching selectively "attacks" these regions of high organic content[1]. In this way, the tablet features that are of key interest in this study were made visible in AFM scans by the outlines left behind by the removal of the organic matrix after surface etching.

First, the nacre sample was immersed in a droplet of ethylenediaminetetraacetic acid (EDTA, 0.5 M) for 15 minutes to partially dissolve the organic matrix. The EDTA was then suctioned off using a pipette, and the sample was gently flushed with tap water, again using a pipette to suction away the excess water. Then, the sample was treated with an aqueous solution of sodium hypochlorite (NaClO, 13 volume % chlorine). The same process was carried out as for the EDTA, using a pipette to suction off excess NaClO, then flushing with tap water. After the etching, the sample was allowed to dry in ambient conditions prior to imaging.

D. Atomic Force Microscopy

In-situ high-resolution AFM imaging with a *Quesant* ® Q-scope 350 AFM of the

surface of the freshly-cleaved nacre sample was performed in ambient conditions prior to nanoindentation, in order to isolate a perfectly flat and clean area for nanoindentation. The indented area was imaged immediately after indentation and once more after etching. AFM specifications and operating parameters are given in the section B of the Appendix.

III. Results

A. Nanoindentation

1 mN—The average elastic modulus for the grid of 256 indents carried out at a maximum load of 1 mN was found to be 97.8 GPa, with a standard deviation of 6.41 GPa. The maximum and minimum moduli values were 115.9 GPa and 81.4 GPa, respectively. The average hardness was found to be 5.41 GPa with a standard deviation of 0.49 GPa. The maximum and minimum hardness values were 6.84 GPa and 4.16 GPa, respectively. The average contact depth was found to be 65.4 nm.

500 μN—The average modulus was found to be 94.8 GPa with a standard deviation of 7.28 GPa. The maximum and minimum moduli values were 122.4 GPa and 65.92 GPa, respectively. The average hardness was found to be 4.89 GPa with a standard deviation of 0.53 GPa. The maximum and minimum hardness values were 6.32 GPa and 3.41 GPa, respectively. The average contact depth was found to be 44.9 nm.

Figure 4 shows the averaged nanoindentation curves for the indents carried out at maximum loads of 1 mN and 500 μN, as well as for a maximum load of 100 μN for purposes of comparison.

B. Atomic Force Microscopy

High-resolution tapping-mode AFM scans reveal the surface morphology of nacre in great detail. Those areas free of debris were used for nanoindentation (Figures 5a and 5b). Scans of the grid of indents were taken before the surface etching treatment (Figures

6a and 6b). The images of the grid of indents after the surface etching treatment reveal the deorganified array of mineral tablets. While in most cases the surface treatment was effective in deorganifying the surface of the nacre in order to clearly expose the tablet features (Figure 7b), in other cases the mineral tablets were removed from the indented region (Figure 7a). Technical and experimental issues are discussed in more detail in Chapter IV Discussion.

C. Mapping

Since for each indent a unique value of elastic modulus and hardness was extracted using the Oliver-Pharr methodology briefly described above, it is possible to plot each of these values of modulus and hardness against the set of x- and y-coordinates for each indent position, using spreadsheet software. In this way, a two-dimensional (or flattened) contour map can be produced that shows the spatial distribution of each property as a function of indent position. For the region between neighboring data points, the software employs a linear interpolation of these data in order to produce a continuous 2-D map of the properties distribution.

Figure 8a shows a map of the 2-D spatial distribution of the elastic modulus as a function of indent position for the grid of indents carried out at a maximum load of 1 mN. The grid size is 30 μm x 30 μm. The x- and y-scales correspond to the positions of individual indents in the grid, and the z-scale is elastic modulus in units of gigapascals (GPa). The grid size is 30 μm x 30 μm. Figure 8b shows a map of the 2-D spatial distribution of the hardness for the same grid of indents carried out at a maximum load of 1 mN.

A map of the 2-D spatial distribution of elastic modulus as a function of indent position for the indents carried out at a maximum load of 500 μN is shown in Figure 9a.

The grid size is 15 μm x 15 μm. . Figure 9b shows a map of the 2-D spatial distribution of the hardness for the same grid of indents carried out at a maximum load of 500 μN.

The AFM images of the etched nacre were used to distinguish the tablet boundaries and sector lines and overlay the traced outlines of these features onto the properties maps (Figures 10 and 11). This was in order to correlate qualitatively the tablet outlines and features with the 2-D spatial properties distribution.

IV. Discussion

A. Nanoindentation and Mapping

As was previously stated, the aim of this investigation was to produce maps of the 2-D properties distribution. As can be seen from the maps that were generated, the properties distribution at this length scale exhibits a high degree of heterogeneity. While regions of uniform modulus and hardness can be seen, noticeable, as well, are distinct and highly-localized areas in which the modulus and hardness deviate substantially from the average nanomechanical modulus and hardness as well as from the continuum values of these properties as they are stated in the literature[9]. It can be seen in all four of the maps that these highly-localized regions occur in close proximity to each other. On the 500 μN map for instance, the nanomechanical properties can vary by up to 50% within less than 2 μm. From the results of nanoindentation, there exists a general trend in the value of the modulus and hardness with low standard deviations from the average. The structure of the nacre would seem to suggest that the larger deviations from the macroscopic elastic modulus are a result of the heterogeneity the topography and the heterogeneity of the composite structure of nacre. The correlation between properties distribution and the position of the indent with respect to tablet features is not immediately apparent. It is prudent to note that the properties distribution for indents carried out in single-crystal

aragonite would yield trivial results as the modulus and hardness of single-crystal aragonite would not be expected to change when indenting along the same crystallographic plane, as was done in these experiments. Were the nanomechanical deformation of nacre similar to that of single-crystal aragonite, i.e. if the structural heterogeneity of nacre had no effect on the mechanical response, we would expect a less marked difference among the values of modulus and hardness at different indent positions. We can reasonable conclude that the heterogeneity of the properties distribution seen in the maps for these experiments seems to be a direct consequence of the role of the heterogeneity of structural features seen in the well-characterized architecture of nacre[1]. Finally, the fact that the mechanical properties can vary widely even within 1 μm, may indicate that the variation mechanical properties is controlled at a smaller length scale, possibly on the length scale of assemblies of nanoasperities, i.e. several hundreds of nanometers. Future studies that are concordant with the question of map resolution are discussed in chapter five.

B. Technical and Experimental Issues

Nanoindentation — The aim of the nanoindentation grids was to indent an entire mineral tablet and the surrounding vicinity. During the development of the experimental protocol several issues arose that had to be addressed in order to optimize the experimental conditions and parameters. Attempts were made to reduce the grid size as much as possible in order to increase the area density of indents and thus the resolution of the mechanical properties maps . Two of the main issues that arose out of the protocol for nanoindentation were indent pile-up and drift of the indenter tip. Firstly, it became apparent in early position-sensitive experiments that the pile-up around indents caused by plastic flow during the deformation of nacre upon indenting was significant enough at low indent spacing to yield inaccurate and unreliable values for the modulus and hardness.

This is because an indent performed in area that is already deformed will yield false values of the mechanical properties since deformation in general alters the mechanical response. Furthermore, since indents carried at different loads tend to differ in contact area and contact depth, different indent spacings were needed for indents carried out at different maximum loads. Consequently, it was necessary to optimize the indent spacing for both the 1 mN and the 500 μN grids of indents.

Moreover, from early indentation in a square grid the disparity between the expected position of an indent and its actual position became even more apparent at low indent spacing. For example, overlapping of indents (often one indent on top of another) and irregular, distorted grids of indents were observed during the early experimental phase. While the Hysitron ® nanoindenter corrects for thermal drift in the piezoelectric tube that actuates the motion of the indenter tip during indentation and while the spatial resolution of the piezo-tube is on the order of a few nanometers (as stated in the Hysitron ® Triboindenter technical manual), a possible reason for the drift may be the fact that the stage upon which samples rest during indentation does not have drift-correction features and is actuated not by piezoelectric actuators but by bearing motors, which have lower spatial resolution. The issue of drift was further exacerbated by the fact that indents were performed in a square grid in which indents had between two and four nearest-neighbor indents.

Finally, a trial-and-error methodology was used to optimize the indent spacing taking into account the constraints of drift, pile-up, proximity of indents, and the objective to indent on a sufficiently small grid to encompass at least one tablet.

Surface Etching — As previously mentioned, the surface etching protocol was developed out of a necessity to reveal the tablet outlines in a repeatable fashion in order to

correlate tablet features with indent position (and ultimately nanomechanical properties). The treatment times needed to be optimized to properly deorganify the surface of the nacre (remove the organic matrix from the tablet and sector boundaries) while preventing the demineralization of the tablets themselves, since EDTA, a chelating agent, and NaClO, a strong base, breakdown both the organic and inorganic components of nacre. The original etching protocol only provided for the use of EDTA to deorganify, but since long treatment times were needed, the protocol was expanded to include treatment with an alkaline compound, aqueous NaClO. While the surface treatment was largely successful in accomplishing said objective, it is not possible to fully control the action of the surface treatment on the nacre aside from changing concentrations of the solutions and the treatment times. Despite the fact that the etching successfully deorganified the nacre, the removal of whole sections of tablets or parts of tablets was observed on isolated occasions (Figure 7b). This may be due to the fact that the surface etching removes the biomacromolecular "mortar" that holds the tablet "bricks" in place thereby causing the tablets to be washed away at times during flushing.

V. Future Studies

The ultimate objective of attaining a complete understanding of the nanomechanical properties distribution would be furthered by a rigorous statistical analysis of the results of this research. In order to fully correlate the properties distribution with indent position and tablet features, and in order to determine the precise nature of that correlation, a full assay of the positions of each indent and their proximity to tablet features of particular significance, such as nucleation sites and tablet sectors, would need to be carried out in order to produce a large set of meaningful statistical data with which to correlate position and mechanical properties quantitatively. The specific type of statistical analysis to

conduct as well as its scope and depth are as-yet undetermined.

Although this research focused on generating a map of the 2-D spatial properties distribution and only qualitatively attempts were made to correlate that distribution to the tablet features, it may be possible to obtain a more palpable qualitative correlation by indenting on a much smaller grid—which would require the maximum indentation load to be much less. A comparison of the properties maps for the two maximum loads shows a distinct qualitative difference in the properties distribution, namely that the map of the 500 μN indents appears to show greater heterogeneity. Likewise, by indenting on a much smaller grid—perhaps fewer than 5 μm x 5μm, e.g. indenting individual nanoasperities—the resolution of the maps would greatly increase and the structure-properties correlation may be more apparent.

VII. Acknowledgements

The author wishes to acknowledge and thank: Associate Professor of Materials Science and Engineering Christine Ortíz, Benjamin J. F. Bruet, Candidate for Ph.D. in Materials Science and Engineering, Alan Schwartzman and the MIT Nanomechanical Technology Laboratory, the MIT Department of Materials Science and Engineering (DMSE), DMSE Professor of Ceramics Bernhardt J. Wuensch, the MIT Institute for Soldier Nanotechnologies (ISN), the MIT Undergraduate Research Opportunities Program (UROP), Cathal Kearney and Kuangshin Tai, Candidates for Ph.D. in Materials Science and Engineering, Thomas Lord Assistant Professor of Materials Science and Engineering Krystyn J. Van Vliet, and Ms. Celia Macias, S.B. '04.

VI. Appendix

A. Nanoindentation

Nanoindentation experiments were conducted in ambient conditions using a

Hysitron, Inc. (Minneapolis, MN) Triboindenter equipped with tapping mode atomic force microscope (TMAFM, Quesant Q-Scope). The instrument is housed in a granite frame environmental isolation chamber so as to minimize instabilities due to the ambient background noise, active piezoelectric vibration control stages (Hysitron, Inc.), and a thermal drift calibration step. The piezoelectric transducer was allowed to equilibrate for 660 seconds (the last 60 seconds with digital feedback) prior to each indent. The drift rate of the transducer was automatically monitored by the software before indentation was initiated. The applied load function was divided into five segments as follows. The first segment consisted of a 3 second hold at zero force allowing for tip-sample equilibration. Segment two was a constant loading rate of 10 μN/sec. Once the maximum set peak load was reached, a third segment which was a hold period of 10 seconds would ensue. The fourth segment decreases the load until reaching zero force with an unloading rate equivalent to that of segment two. The fifth segment would conclude the experiment with a 50 second hold at zero force, in order to calculate the final drift rate of the piezo. The probe tip area function ($^{A(}h_c$) which is the projected area of the Berkovich probe tip under load calculated from a 6th order polynominal fit accounting for nonideal tip geometry as a function of the contact depth, h_c) and frame compliance were calibrated prior to each set of experiments using a fused quartz sample[†].

B. Atomic Force Microscopy

In-situ high-resolution AFM imaging was carried out on the nacre using a *Quesant* Q-scope 350 AFM (attached to the *Hysitron, Inc.* Triboindenter nanoindenter) in tapping mode with a piezoelectric tube scanning element (X-Y scan range ~40 μm, vertical Z limit ~4.5 μm) and Si_3N_4 Wavemode NSC16 cantilevers (rectangular shaped with conical probe tip geometry, $l \sim 230$ μm, width ~ 40 μm, cone angle < 20°, probe tip height ~ 15-20 μm,

resonance frequency, ω ~170 kHz, k ~ 40 N/m, and R_{TIP} ~10 nm). A scan rate of 2 Hz using a maximum sample size of 512 x 512 pixels was employed. The drive amplitude and amplitude set-point (~0.25 V) were optimized prior to imaging and gains between 350 and 550 were employed[1†].

C. The Oliver-Pharr Analysis Method

1 The procedure used to determine the reduced Young's Modulus E_r and the Hardness H of the material from nanoindentation curves is described below. the portion of the unloading curve between 95 and 20 % of the maximum load to is fit to the power law relation,

$$2P = B(h - h_{max})^m$$

where

P is the load
B is a constant to be determined
h is the indentation depth
h_{max} is the maximal indentation depth
m is a constant to be determined

The derivative of the power law relation with respect to h is evaluated at the maximum load to calculate the contact stiffness S,

$$S = \left(\frac{dP}{dh}\right)_{h_{max}}$$

The contact depth, h_c, is calculated with the following equation:

$$h_c = h_{max} - \frac{3P_{max}}{4S}$$

The hardness H is calculated with:

$$H = \frac{P_{max}}{A(h_c)}$$

where $A(h_c)$ is the projected contact area of the tip at the height . Practically, the area function is calibrated before each set of experiments (see below).

3

The reduced modulus (see definition below) is calculated with:

$$E_r = \frac{\sqrt{\pi}}{2\sqrt{A(h_c)}} S$$

Tip-shape calibration is based on determining the area function of the indenter tip. The method is based on the assumption that Young's modulus of elasticity is constant and independent of indentation depth. Fused quartz with reduced Young's modulus of 69.6 GPa is used as a standard sample for calibration purpose. An area function relating the projected contact area (A) to the contact depth (h_c) is obtained. For an ideal pyramidal geometry Berkovich tip, the projected contact area to depth relationship is given by:

$$A(h_c) = 24.5 h_c$$

In the general case,

$$A(h_c) = \frac{\pi}{4}\left(\frac{S}{E_r}\right)^2$$

where the reduced modulus E_r accounts for the fact that the measured displacement includes contribution from both the specimen and the indenter. The reduced modulus is given by:

$$\frac{1}{E_r} = \left(\frac{1-\nu^2}{E}\right)_{specimen} + \left(\frac{1-\nu^2}{E}\right)_{indenter}$$

where E and ν are the elastic modulus and Poisson's ratio of the specimen and the indenter respectively.

To determine the area function, a series of indents at various contact depths (normal

loads) are performed on fused quartz specimen and the contact area (A) calculated using the general equation above A plot of the computed area as a function of contact depth is plotted and a fitting procedure is employed to fit the (A) versus (hc) to a sixth order polynomial of the form:

$$A(h_c) = C_0 h_c^2 + C_0 h_1 + C_0 h_2^{1/2} + C_0 h_3^{1/4} + C_0 h_4^{1/8} + C_0 h_5^{1/16}$$

Adapted from TriboScope® Users Manual, © 2003 Hysitron Inc.

VIII. References

1. B.J.F. Bruet, H.J. Qi, M.C. Boyce, R. Panas, K. Tai, L. Frick, and C. Ortiz: Nanoscale morphology and indentation of individual nacre tablets from the gastropod mollusk Trochus Niloticus. J. Mater. Res. **20** (9), 2400 (2005). (†reprinted with permission)
2. National Materials Advisory Board, Committee on Synthetic Hierarchical Structures. Hierarchical Structures in Biology as a Guide for New Materials Technology. National Academy Press, National Academy of Science: Washington, D.C.; 1994
3. H. K. Erban: On the structure and growth of the nacreous tablets in gastropods. Biomineralisation **4**, 14 (1972).
4. J. D. Taylor, W. J. Kennedy, and A. Hall: Shell structure and minerology of the bivalvia: Introduction Nuculacea-Rrigonacea. Bull. Br. Mus. nat. Hist. Zool. **Suppl. 3**, 1 (1969).
5. H. Mutvei: Ultrastructural characteristics of the nacre in some gastropods. Zool. Scr. **7**, 287 (1978).
6. D. Chateigner, C. Hedegaard, H.-R. Wenk: Mollusc shell microstructures and crystallographic textures. J. Struc. Geol. **22**, 1723 (2000).
7. Y. Zhang, L. Xie, Q. Meng, T. Jiang, R. Pu, L. Chen, and R. Zhang: A novel matrix protein participating in the nacre framework formation of pearl oyster, *Pinctada fucata*. Comp. Biochem. Physiol. B. Biochem. Mol. Biol. **135** (3), 565 (2003).
8. X. Li, W.-C. Chang, Y. J. Chao, R. Wang, and M. Chang: Nanoscale structural and mechanical characterization of a natural nanocomposite material : The shell of red abalone. Nano Lett. **4**(4), 613 (2004).
9. A. P. Jackson, J. F. V. Vincent, and R. M. Turner: The mechanical design of nacre. Proc. Roy. Soc. London, Series B **234**, 415 (1988).
10. R. Z. Wang, Z. Suo, A. G. Evans, N. Yao, and I. A. Aksay: Deformation mechanisms in nacre. J. Mater. Res. **16**(9), 2485 (2001).
11. Handbook of elastic properties of solids, liquids and gases, editors-in-chief, M. Levy, H. Bass, R. Stern ; volume editors, A. G. Every, W. Sachse. (2001)
12. W. C. Oliver and G. M. Pharr: An improved technique for determining hardness and elastic modulus using load and displacement sensing indentation experiments. J. Mater. Res. **7**, 1564 (1992).

IX. Figures

Figure 1.

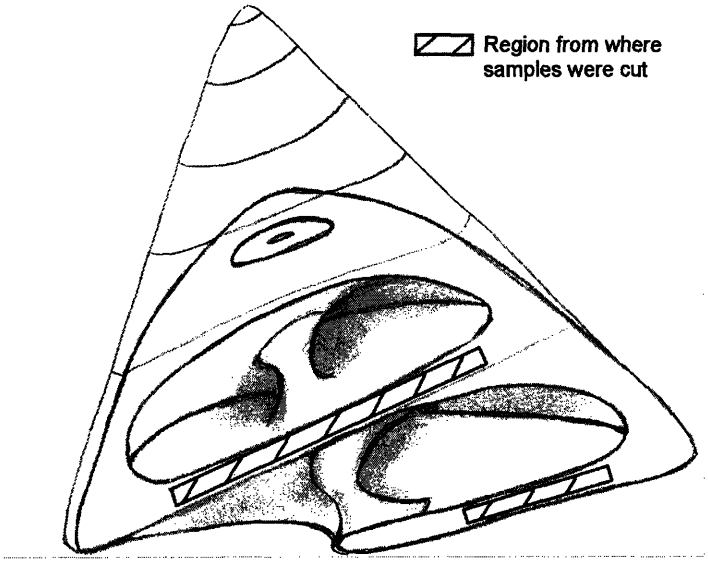

B.J.F. Bruet, et al., J. Mater. Res. **20** (9), 2400 (2005).

Figure 2.

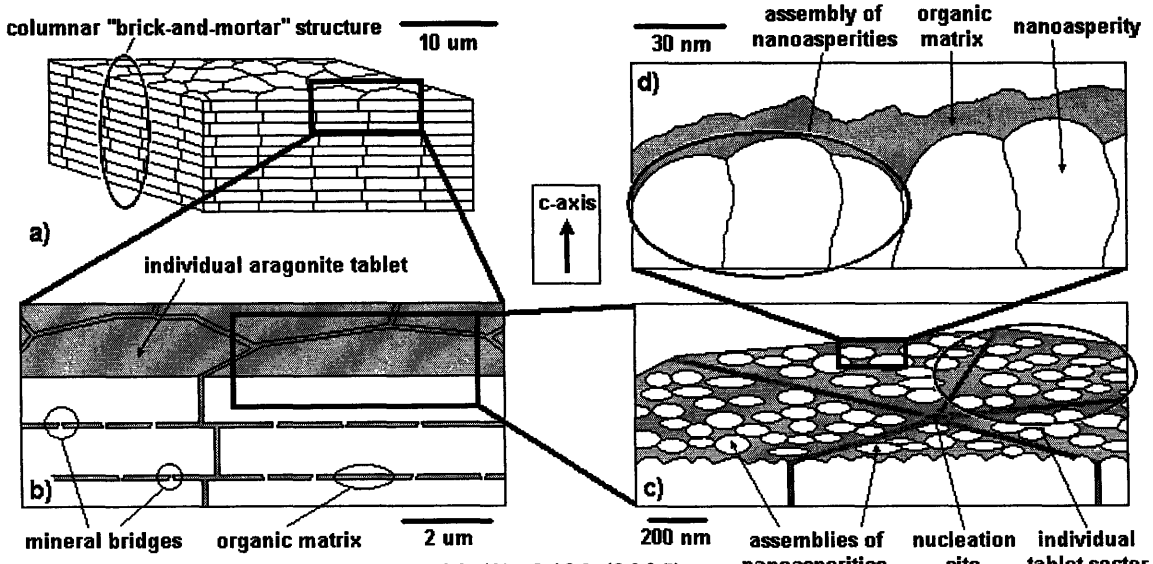

B.J.F. Bruet, et al., J. Mater. Res. **20** (9), 2400 (2005).

Figure 3 .

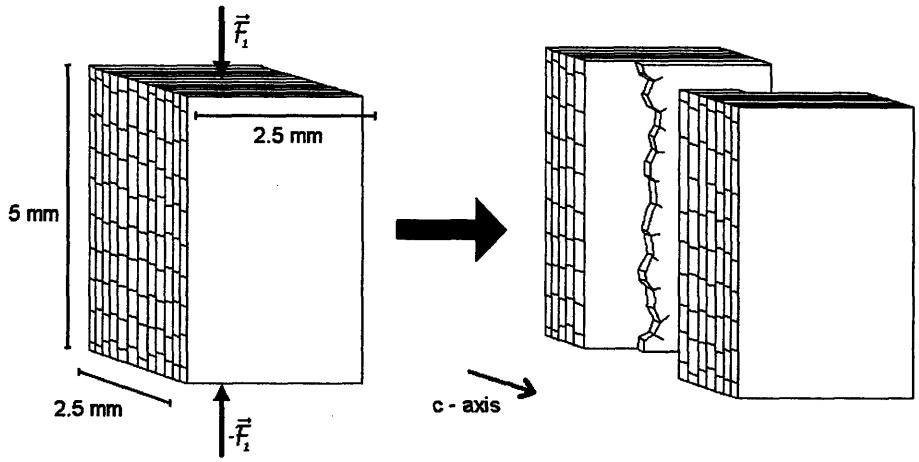

B.J.F. Bruet, et al., J. Mater. Res. **20** (9), 2400 (2005).

Figure 4.

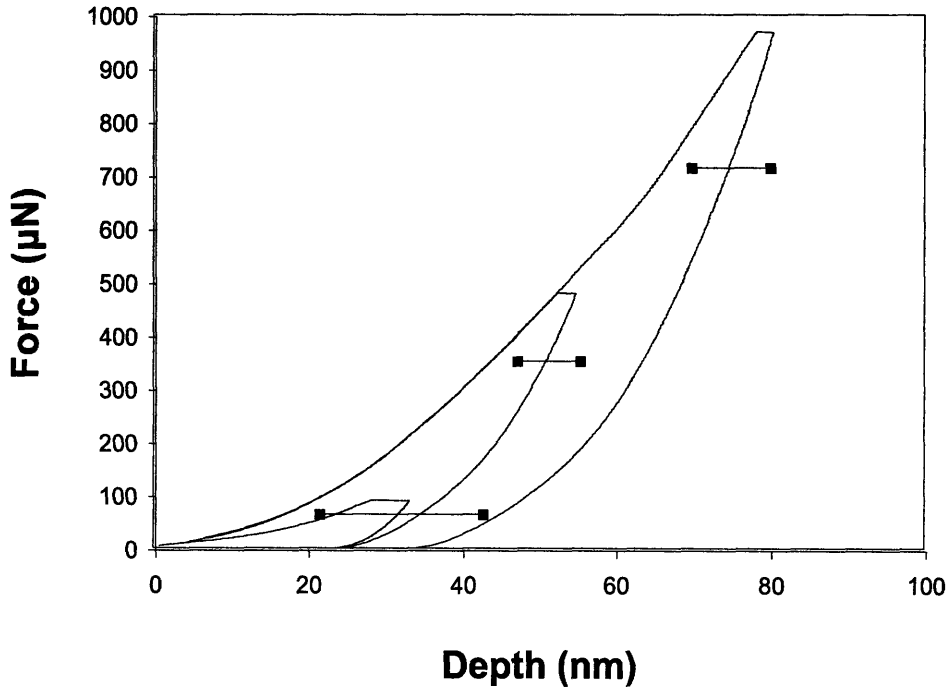

Figure 5a.

Figure 5b.

Figure 6a.

Figure 6b.

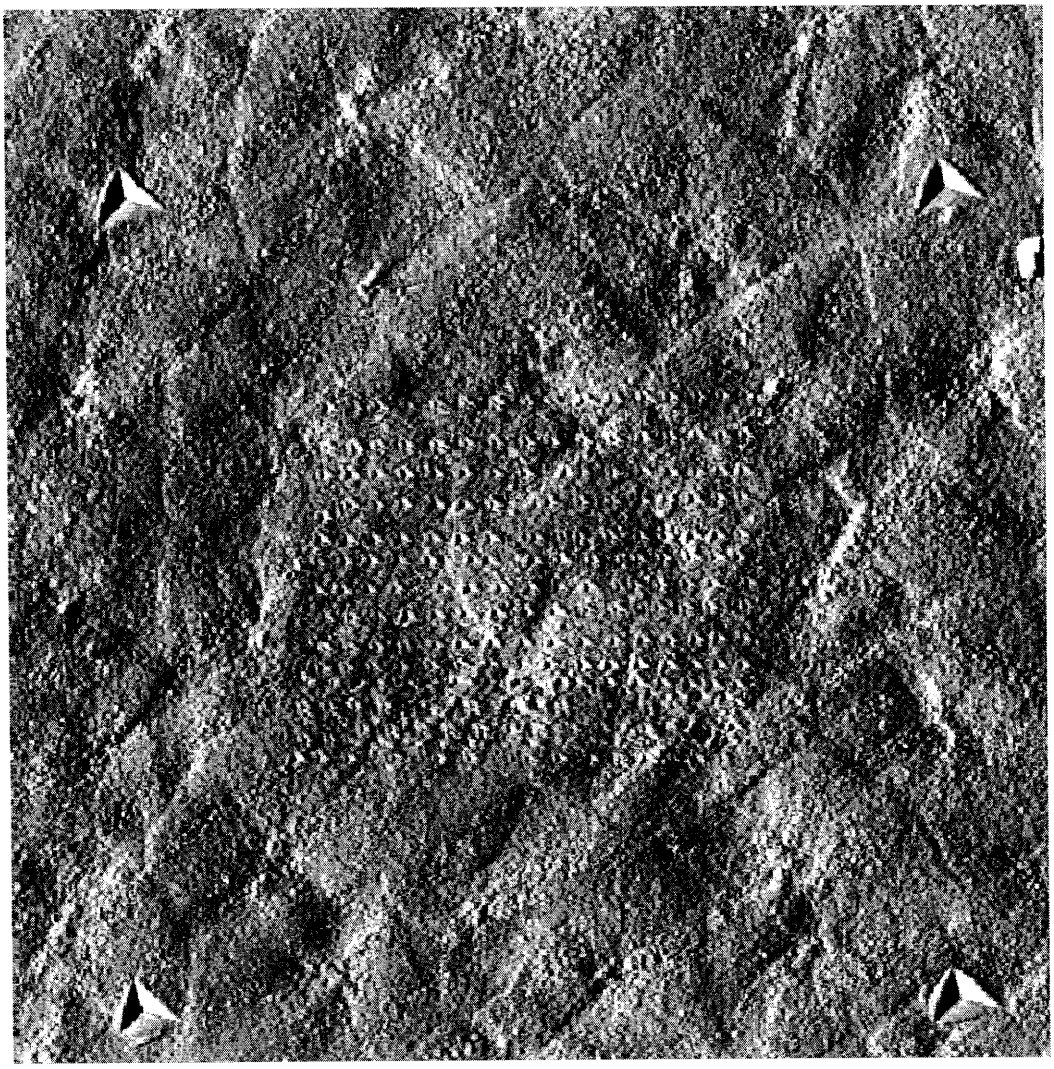

Figure 7a.

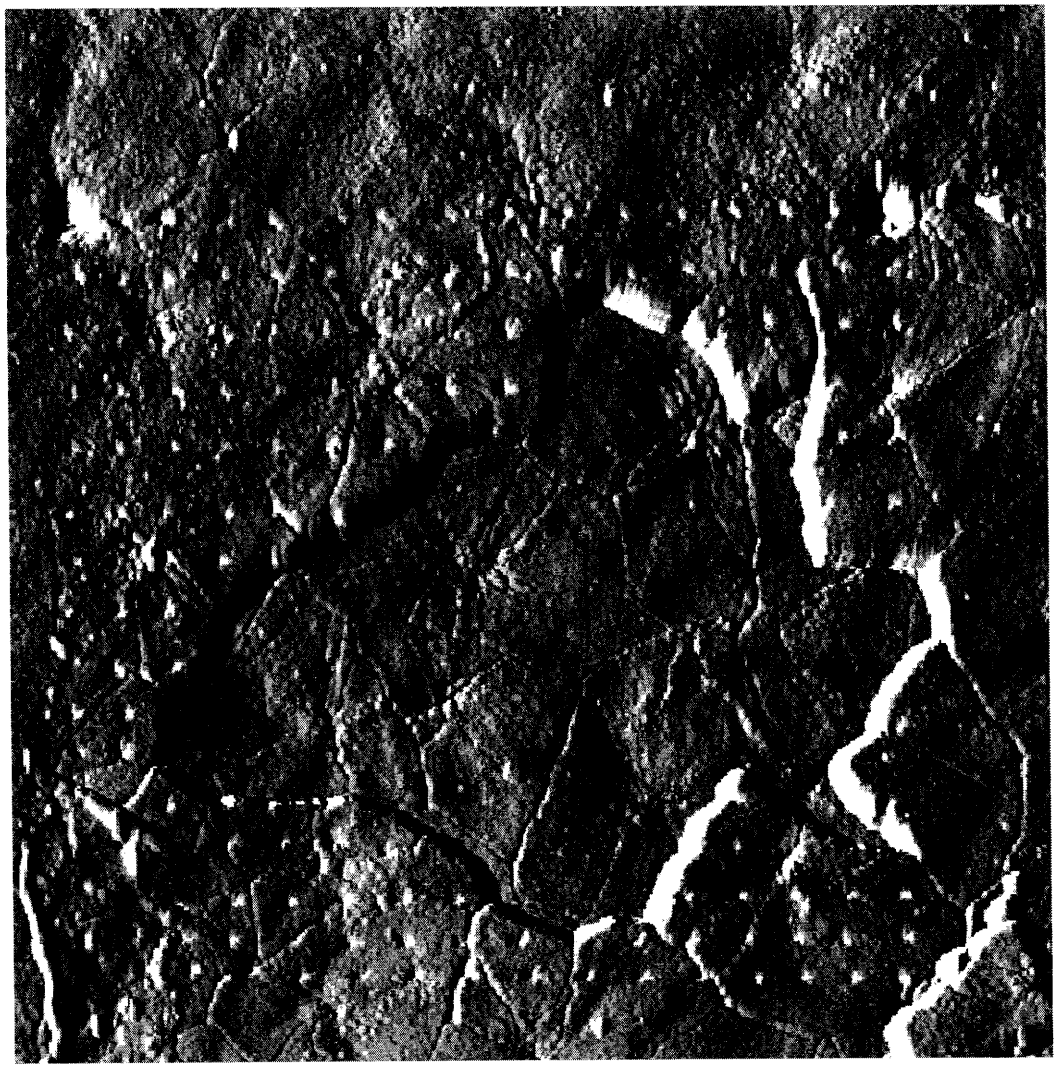

Figure 7b.

Figure 8a.

Elastic Modulus (GPa)

- 111-114
- 108-111
- 105-108
- 102-105
- 99-102
- 96-99
- 93-96
- 90-93
- 87-90
- 84-87
- 81-84

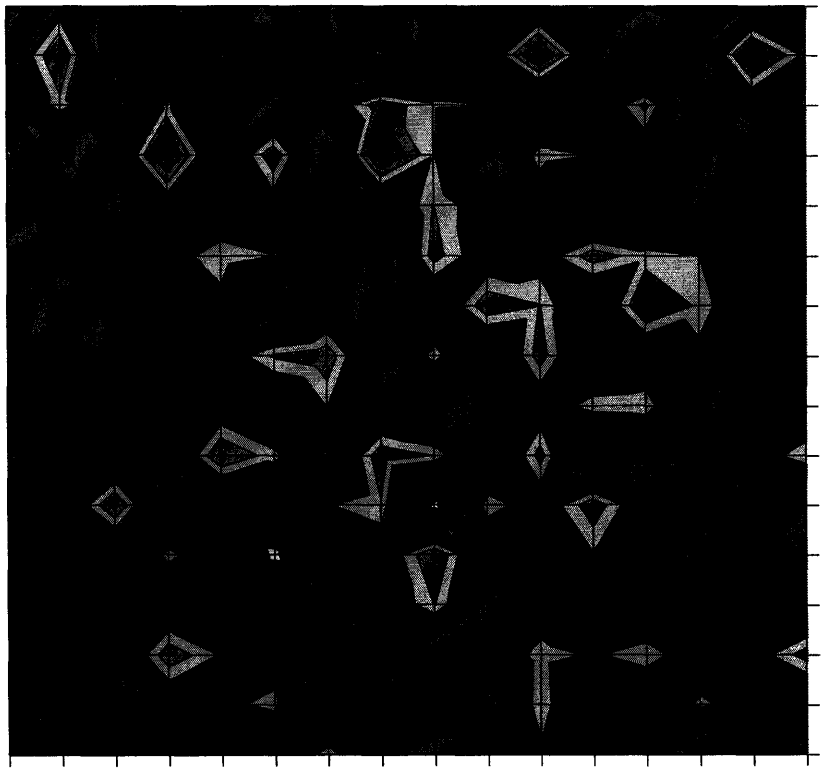

Figure 8b.

Hardness (GPa)

- 6.8-7
- 6.6-6.8
- 6.4-6.6
- 6.2-6.4
- 6-6.2
- 5.8-6
- 5.6-5.8
- 5.4-5.6
- 5.2-5.4
- 5-5.2
- 4.8-5
- 4.6-4.8
- 4.4-4.6
- 4.2-4.4
- 4-4.2

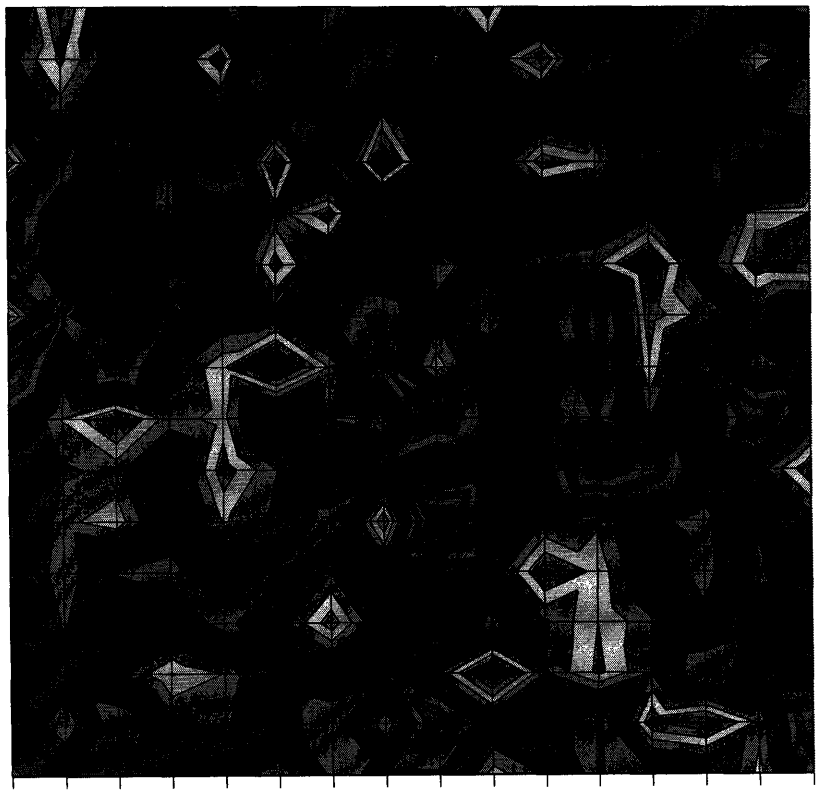

Figure 9a.

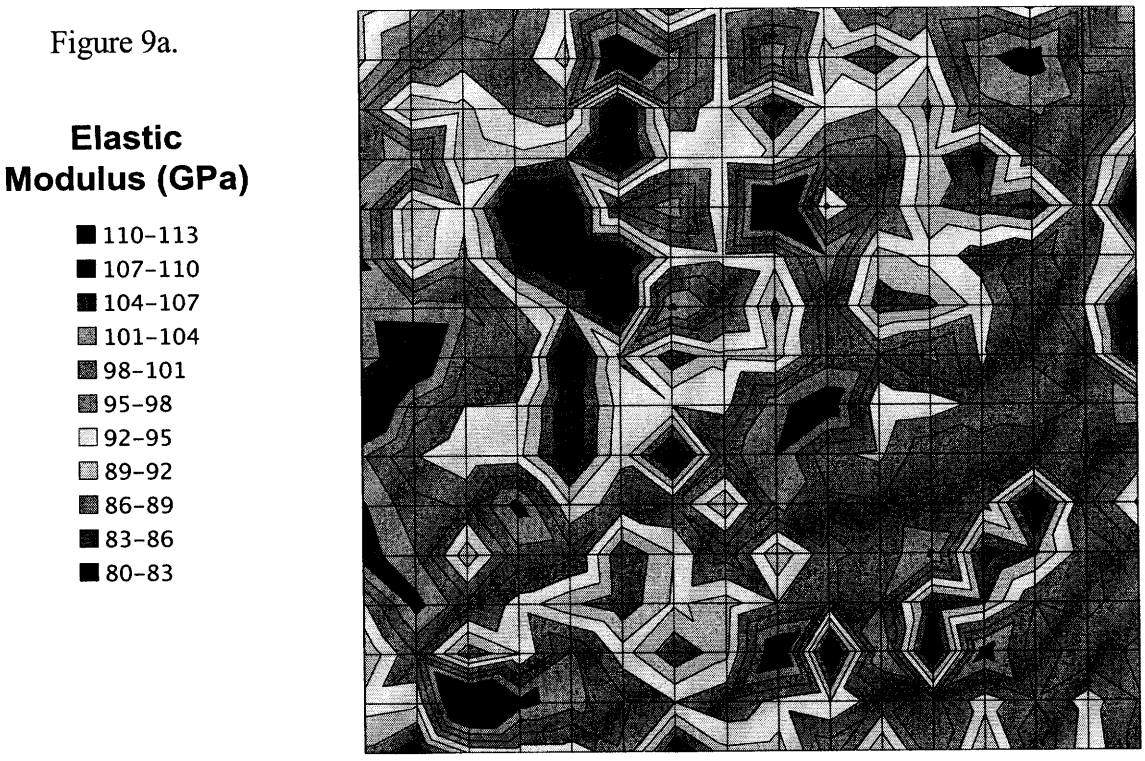

Figure 9b.

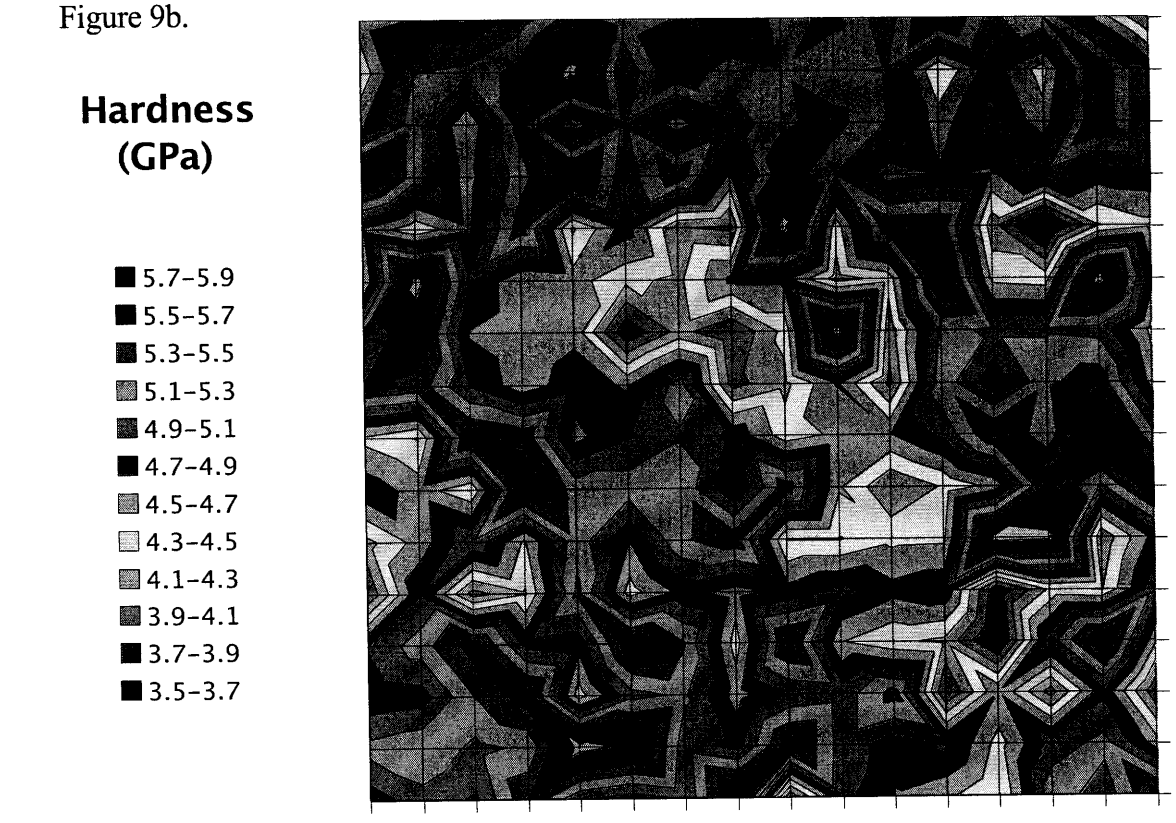

Figure 10a.

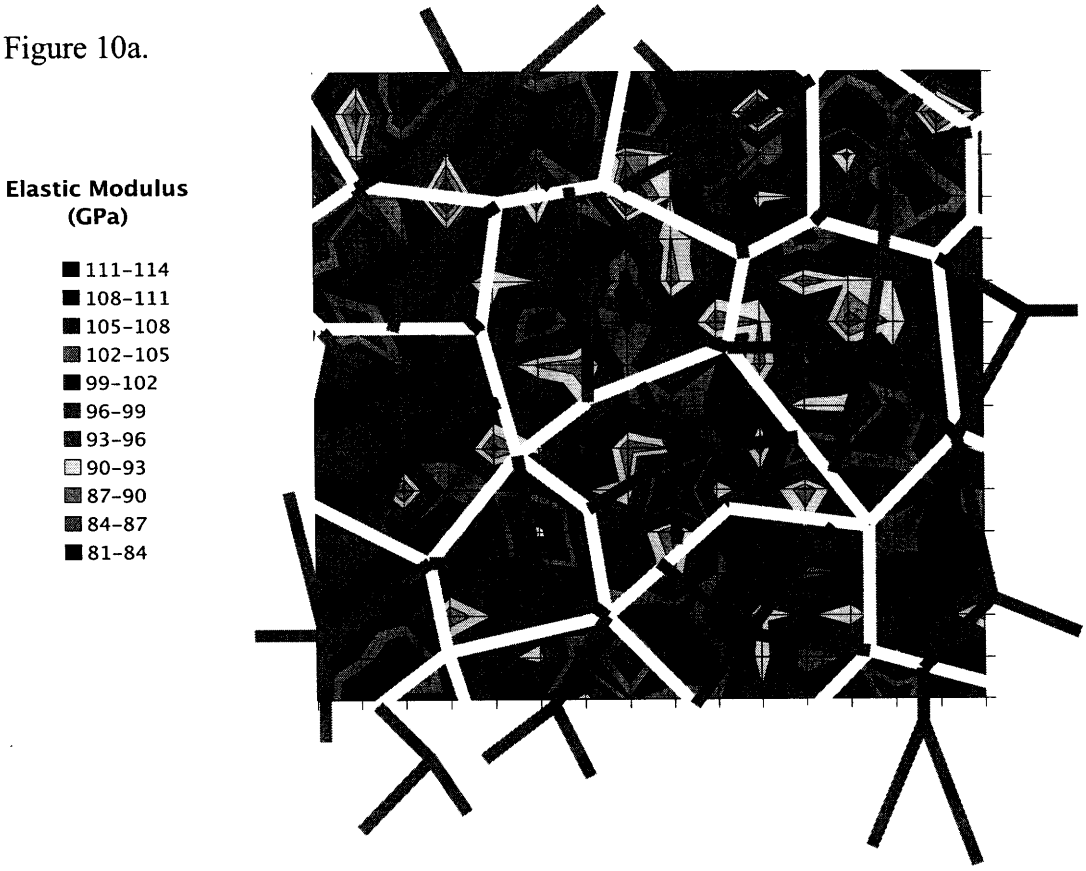

Figure 10b.

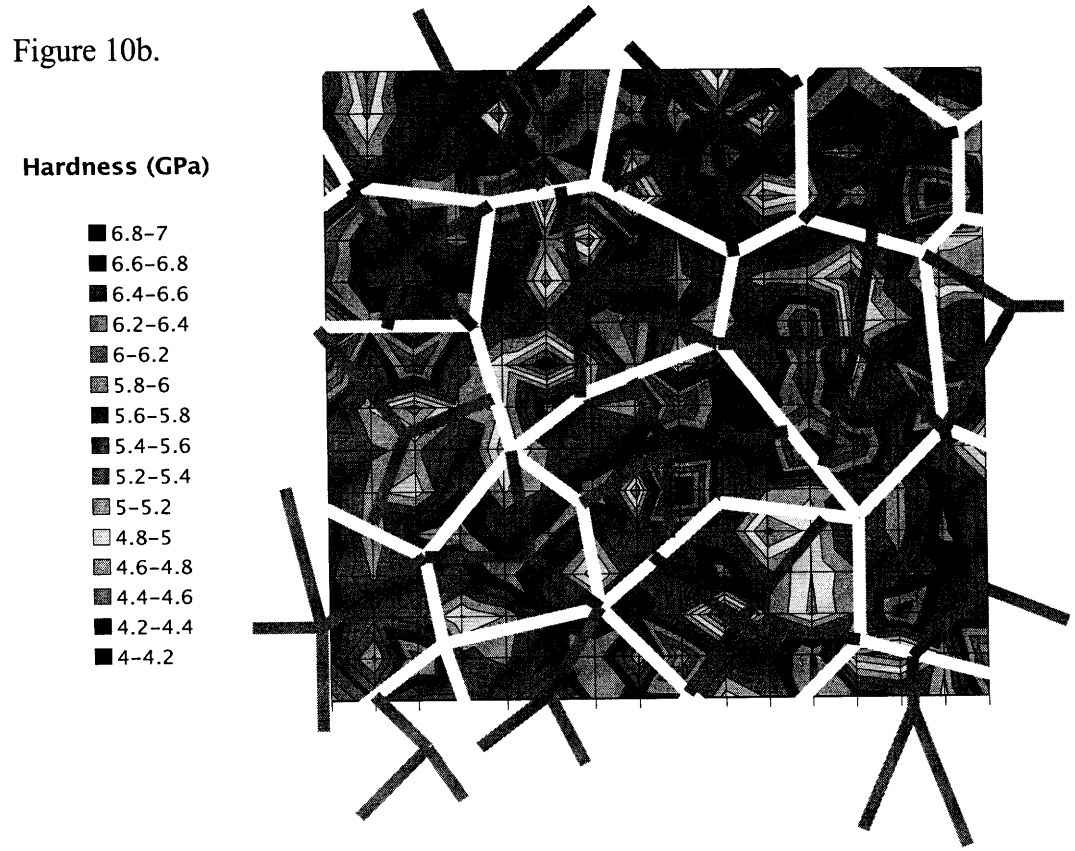

Figure 11a.

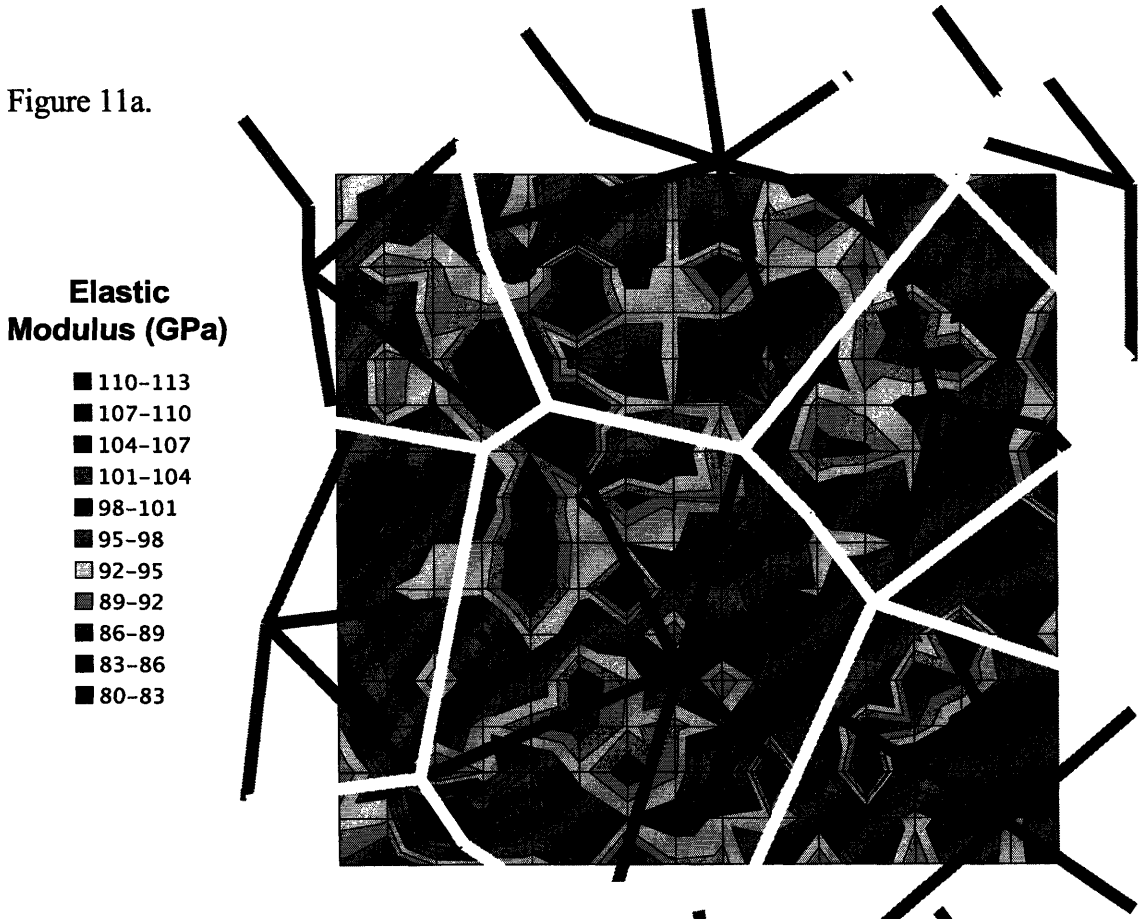

Figure 11b.

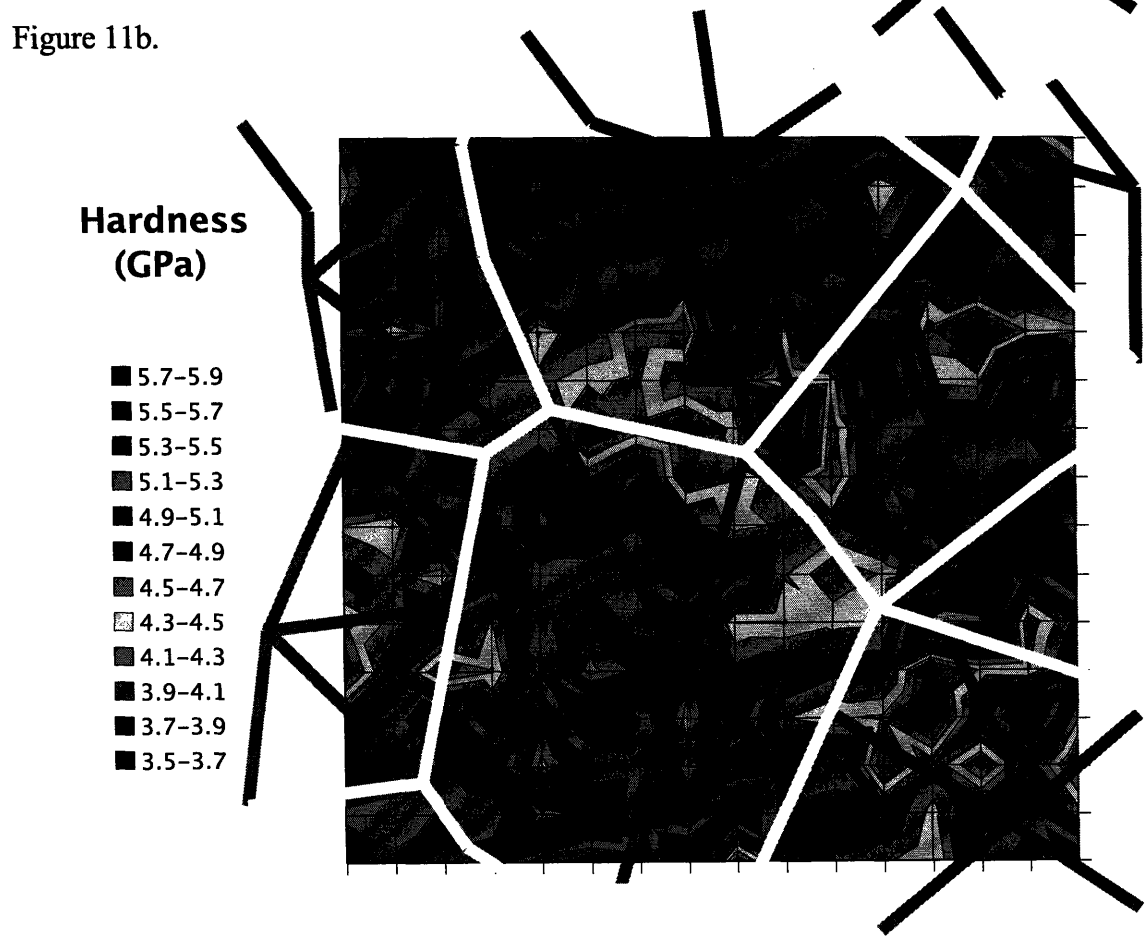

X. Figure Captions

Figure 1: This sketch of a full-sized *Trochus niloticus* shell shows where the nacreous layer is found.

Figure 2: The hierarchical structure of nacre can be seen in this diagram. Magnification increases counterclockwise from the upper left.

Figure 3: A diagram of a nacre sample being cleaved in uniaxial compression. The axis of loading is oriented perpendicular to the aragonite c-axis.

Figure 4: A graph of the averaged nanoindentation curves shows the general shape of the Force vs. Displacement depth curves and the standard deviations for experiments carried out a maximum loads of 1 mN (1000 μN), 500 μN, and 100 μN.

Figure 5a: 1 mN – Amplitude AFM image in tapping mode of the surface of freshly-cleaved nacre before nanoindentation, 40 μm x 40 μm scan size.

Figure 5b: 500 μN – Amplitude AFM image in tapping mode of the surface of freshly-cleaved nacre before nanoindentation, 40 μm x 40 μm scan size.

Figure 6a: 1 mN – Amplitude AFM image in tapping mode of the grid of 256 indents, 40 μm x 40 μm scan size.

Figure 6b: 500 μN – Amplitude AFM image in tapping mode of the grid of 256 indents, 40 μm x 40 μm scan size.

Figure 7a: 1 mN – Amplitude AFM image in tapping mode of the grid of indents after surface etching.

Figure 7b: 500 μN – Amplitude AFM image in tapping mode of the grid of indents after surface etching.

Figure 8a: 1 mN – Map of the 2-D spatial distribution of elastic modulus as a function of indent position, 30 μm x 30 μm grid size.

Figure 8b: 1 mN – Map of the 2-D spatial distribution of hardness as a function of indent position, 30 μm x 30 μm grid size.

Figure 9a: 500 μN – Map of the 2-D spatial distribution of elastic modulus as a function of indent position, 15 μm x 15 μm grid size.

Figure 9b: 500μN – Map of the 2-D spatial distribution of hardness as a function of indent position, 15 μm x 15 μm grid size.

Figure 10a: 1 mN – Tablet boundaries overlain onto map of the elastic modulus distribution, 30 μm x 30 μm grid size.

Figure 10b: 1 mN – Tablet boundaries overlain onto map of the hardness distribution, 30 μm x 30 μm grid size.

Figure 11a: 500 μN – Tablet boundaries overlain onto map of the elastic modulus distribution, 15 μm x 15 μm grid size.

Figure 11b: 500 μN – Tablet boundaries overlain onto map of the hardness distribution, 15 μm x 15 μm grid size.